

Exploring the phase structure of lattice QCD with twisted mass quarks*

F. Farchioni^a, C. Urbach^{bc}, R. Frezzotti^d, K. Jansen^b, I. Montvay^e, G.C. Rossif, E.E. Scholz^e,
A. Shindler^b, N. Ukita^e, I. Wetzorke^b

^aInstitut für Theoretische Physik, Universität Münster, Wilhelm-Klemm-Str.9, D-48149 Münster, Germany

^bNIC/DESY Zeuthen, Platanenallee 6, D-15738 Zeuthen, Germany

^cFreie Universität Berlin, Institut für Theoretische Physik, Arnimallee 14, D-14196 Berlin, Germany

^dINFN, Sezione di Milano and Dipartimento di Fisica, Università di Milano “Bicocca”, Piazza della Scienza 3, I-20126 Milano, Italy

^eDeutsches Elektronen-Synchrotron DESY, Notkestr. 85, D-22603 Hamburg, Germany

^fDipartimento di Fisica, Università di Roma “Tor Vergata” and INFN, Sezione di Roma 2, Via della Ricerca Scientifica, I-00133 Roma, Italy

The phase structure of zero temperature twisted mass lattice QCD is investigated. We find strong metastabilities in the plaquette observable when the untwisted quark mass sweeps across zero.

1. Introduction

In the process of approaching in lattice QCD the physical point, at which the pion mass assumes its value as measured in experiment, the simulation algorithms suffer from a substantial slowing down [1,2] which restricts present simulations to rather high and unphysical values of the quark mass. Moreover the usual Wilson-Dirac operator develops unphysical small eigenvalues at small values of the quark mass which render the simulations more difficult and sometimes even impossible.

An elegant way out may be the use of Wilson twisted mass fermions [3] with the following fermionic action for $N_f = 2$ mass degenerate flavors of quarks in the so called twisted basis (χ)

$$S[\chi, \bar{\chi}, U] = \bar{\chi}(D[U] + m_0 + \mu i\gamma_5\tau^3)\chi, \quad (1)$$

where $D[U]$ is the standard Wilson-Dirac operator, m_0 is the untwisted quark mass parameter, μ is the twisted quark mass parameter and τ^3 is the

third Pauli matrix acting in flavor space. In the present paper, unless otherwise stated, the lattice spacing is set to unity: $a = 1$. The twisted mass μ serves as a natural infrared regulator for the low lying eigenvalues of the Wilson twisted mass operator since

$$\begin{aligned} \det(D[U] + m_0 + \mu i\gamma_5\tau^3) \\ = \det((D[U] + m_0)(D[U] + m_0)^\dagger + \mu^2). \end{aligned} \quad (2)$$

Note that on the l.h.s. the operator is the two flavor operator, while on the r.h.s. $D[U] + m_0$ is only the one flavor part. As for the gauge action, the usual Wilson plaquette action is used. Note that the bare quark mass m_0 is often represented by the hopping parameter κ defined as $\kappa = (2m_0 + 8)^{-1}$.

In addition to the infrared cut-off the Wilson twisted mass formulation allows to get full $O(a)$ improvement for correlation functions and derived quantities with no need of additional counterterms [4,5], provided m_0 is set to its critical value m_{crit} and the value of μ is kept constant as $a \rightarrow 0$.

*Presented by C. Urbach and F. Farchioni.

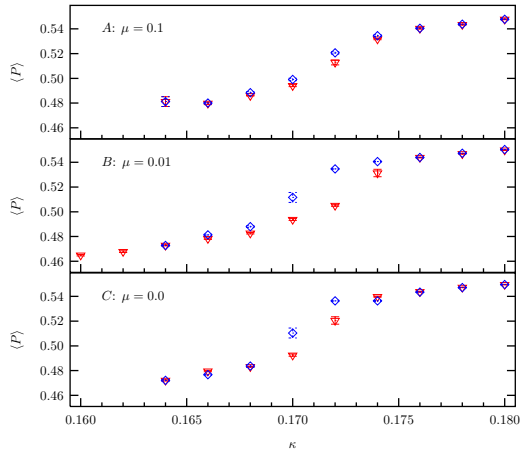


Figure 1. Thermal cycles in κ on $8^3 \times 16$ lattices at $\beta = 5.2$. The plaquette expectation value is shown for: $\mu = 0.1$ (A); $\mu = 0.01$ (B); $\mu = 0$ (C). The triangles refer to increasing κ -values, the diamonds to decreasing ones.

Studying the phase structure of lattice QCD should be a pre-requisite before starting to extract physical results. Indeed, in simulations of $N_f = 3$ clover improved Wilson fermions [6] and of $N_f = 2$ non-perturbatively improved Wilson fermions [2] metastabilities and hysteresis effects were found. In this contribution, or in more detail in [7], we discuss results for the phase structure of $N_f = 2$ Wilson twisted mass fermions.

For our simulations of full QCD we have implemented two independent algorithms: The Two-Step Multi-Boson algorithm (TSMB) and the Hybrid Monte Carlo algorithm (HMC), both with even-odd preconditioning. For the HMC we use in addition the Hasenbusch trick [8]. We checked that we get the same results with both algorithms.

We have performed simulations primarily at $\beta = 5.2$, but we also have some data at $\beta = 5.3$ and $\beta = 5.4$. The lattice sizes are $8^3 \times 16$, $12^3 \times 24$ and $16^3 \times 32$.

2. Thermal cycles and metastable states

We started our investigation of the phase diagram by performing thermal cycles in κ . Fixing

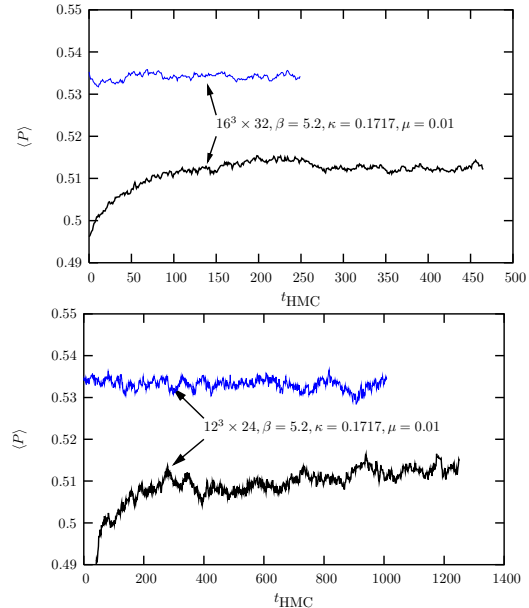


Figure 2. Monte Carlo history of metastable states at $\beta = 5.2$, $\mu = 0.01$ and $\kappa = 0.1717$. In the upper plot the lattice size is $16^3 \times 32$ and in the lower plot it is $12^3 \times 24$.

the values of $\beta = 5.2$ and μ we incremented κ from a starting value κ_{start} until the final value κ_{final} was reached and then reversed the procedure. At each value of κ 150 configurations were produced – without performing further intermediate thermalization sweeps – and averaged over.

In fig. 1 we show three such thermal cycles, performed at $\mu = 0$, $\mu = 0.01$ and $\mu = 0.1$ from bottom to top. In the cycles signs of hysteresis effects can be seen for $\mu = 0$ and $\mu = 0.01$ while for the largest value of $\mu = 0.1$ such effects are hardly visible. Hysteresis effects in thermal cycles *may be* signs of the existence of a first order phase transition. However, they should only be taken as first indications.

Guided by the results from the thermal cycles, we next performed simulations at fixed values of μ and κ , starting with ordered and disordered configurations, staying again at $\beta = 5.2$.

In fig. 2 we show the Monte Carlo time evolution of the plaquette expectation value for two

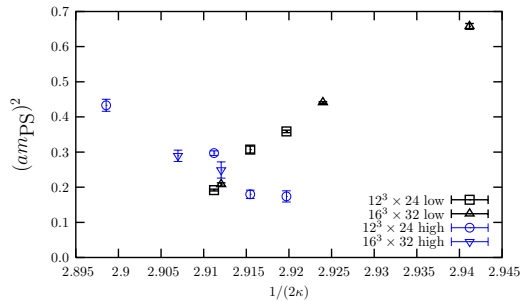


Figure 3. Pseudoscalar mass as a function of $1/(2\kappa)$ at $\beta = 5.2$ and $\mu = 0.01$.

sets of parameters at $\beta = 5.2$. In the upper plot the lattice size is $16^3 \times 32$ and in the lower plot the lattice size $12^3 \times 24$, both with $\mu = 0.01$ and $\kappa = 0.1717$. We find coexisting branches with different values of the average plaquette with a rather large gap in between. As can be seen the gap is not decreasing with increasing lattice size and therefore this behavior cannot be ascribed to any finite volume effect. Furthermore we observed this phenomenon in simulations with $\mu = 0$ and with both algorithms. We therefore conclude that the existence of metastable states is a generic feature of lattice QCD in this formulation.

3. Pseudoscalar and quark masses

In order to study the physical properties in the two metastable states we measured the (charged) pseudoscalar meson mass and the untwisted PCAC quark mass. We obtained the pseudoscalar mass from the pseudoscalar correlation function in the χ -basis while we measured the untwisted PCAC quark mass from the axialvector current in the χ -basis:

$$m_{\chi}^{\text{PCAC}} \equiv \frac{\langle \partial_{\mu}^* \bar{\chi} \gamma_{\mu} \gamma_5 \frac{\tau^{\pm}}{2} \chi(x) \hat{O}^{\mp}(y) \rangle}{2 \langle \bar{\chi} \frac{\tau^{\pm}}{2} \gamma_5 \chi(x) \hat{O}^{\mp}(y) \rangle}. \quad (3)$$

Here \hat{O}^{\mp} is a suitable operator that we have chosen to be the pseudoscalar density $\hat{O}^{\mp} = \bar{\chi} \frac{\tau^{\mp}}{2} \gamma_5 \chi(x)$, ∂_{μ}^* is the lattice backward derivative defined as usual and $\tau^{\pm} = \tau_1 \pm i\tau_2$. One can show that in the continuum limit $a \rightarrow 0$ the

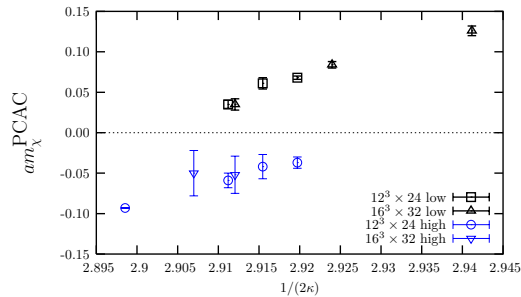


Figure 4. m_{χ}^{PCAC} as a function of $1/(2\kappa)$ at $\beta = 5.2$ and $\mu = 0.01$.

quantity m_{χ}^{PCAC} is asymptotically proportional to $m_0 - m_{\text{crit}}$.

In fig. 3 we show the pseudoscalar mass in lattice units as function of $1/(2\kappa)$. We observe that the “pion” mass is rather large and the most striking effect in the graph is that it can have two different values at the same κ . If we consider the quark mass m_{χ}^{PCAC} in fig. 4, we see that in the phase with a low plaquette expectation value the mass is positive while for high values of the plaquette expectation it is negative. Values of m_{χ}^{PCAC} with opposite sign coexist for some values of κ . From this fact one can safely argue that the value of $1/(2\kappa_{\text{crit}})$ lies between 2.91 and 2.92.

Figures 2-4 clearly reveal that for $\mu = 0.01$ metastabilities show up in the quantities we have investigated, such as m_{PS} , m_{χ}^{PCAC} and the average plaquette, if m_0 is close to its critical value.

4. Determination of the twist angle

The knowledge of the twist angle ω , the polar angle in the plane of the untwisted and twisted mass, is important e.g. when comparing lattice data with analytical predictions [9] from Wilson chiral perturbation theory (WChPT). We present here a method which allows to determine the twist angle only on the basis of symmetry.

Following [3], we introduce² the twist angle ω as the chiral rotation angle between the renormalized (physical) chiral currents \hat{V}_{μ}^a , \hat{A}_{μ}^a and the bare bilinears of the χ -fields V_{μ}^a , A_{μ}^a with renor-

²In [3] this definition of the twist angle was called α .

malization constants Z_V and Z_A . Thus we have

$$\hat{V}_\mu^a = Z_V V_\mu^a \cos \omega + \epsilon_{ab} Z_A A_\mu^b \sin \omega \quad (4)$$

$$\hat{A}_\mu^a = Z_A A_\mu^a \cos \omega + \epsilon_{ab} Z_V V_\mu^b \sin \omega, \quad (5)$$

where only charged currents are considered ($a=1,2$). The twist angle ω is related to the ratio of the renormalized twisted and untwisted masses entering the chiral Ward identities [3]:

$$\omega = \arctan(\mu_R/m_R). \quad (6)$$

We define in addition the two auxiliary angles

$$\omega_V = \arctan(Z_A Z_V^{-1} \tan \omega), \quad (7)$$

$$\omega_A = \arctan(Z_V Z_A^{-1} \tan \omega). \quad (8)$$

In terms of ω_V, ω_A eqs. (4), (5) are written

$$\hat{V}_\mu^a = \mathcal{N}_V (\cos \omega_V V_\mu^a + \epsilon_{ab} \sin \omega_V A_\mu^b) \quad (9)$$

$$\hat{A}_\mu^a = \mathcal{N}_A (\cos \omega_A A_\mu^a + \epsilon_{ab} \sin \omega_A V_\mu^b), \quad (10)$$

where the overall multiplicative renormalization reads

$$\mathcal{N}_X = \frac{Z_X}{\cos \omega_X \sqrt{1 + \tan \omega_V \tan \omega_A}}. \quad (11)$$

From (7), (8) it follows:

$$\omega = \arctan(\sqrt{\tan \omega_V \tan \omega_A}). \quad (12)$$

ω_V and ω_A can be directly determined by imposing parity conservation for suitable matrix elements; e.g., with $P^\pm(x) = \bar{\chi} \frac{\tau^\pm}{2} \gamma_5 \chi(x)$:

$$\sum_{\vec{x}, \vec{y}} \langle \hat{A}_0^+(x) \hat{V}_0^-(y) \rangle = \sum_{\vec{x}, \vec{y}} \langle \hat{V}_0^+(x) P^-(y) \rangle = 0. \quad (13)$$

These equations admit the solution

$$\begin{aligned} \tan \omega_A &= \frac{i \sum_{\vec{x}, \vec{y}} \langle A_0^+(x) V_0^-(y) \rangle + \tan \omega_V \sum_{\vec{x}, \vec{y}} \langle A_0^+(x) A_0^-(y) \rangle}{\sum_{\vec{x}, \vec{y}} \langle V_0^+(x) V_0^-(y) \rangle - i \tan \omega_V \sum_{\vec{x}, \vec{y}} \langle V_0^+(x) A_0^-(y) \rangle} \\ \tan \omega_V &= \frac{-i \sum_{\vec{x}, \vec{y}} \langle V_0^+(x) P^-(y) \rangle}{\sum_{\vec{x}, \vec{y}} \langle A_0^+(x) P^-(y) \rangle}. \end{aligned} \quad (14)$$

Alternatively, a determination of ω_V and ω_A is given by the vector and axialvector Ward identities, respectively; e.g. in the vector

case, by enforcing the Ward identity with the insertion of some appropriate operator $\hat{O}(x)$: $\langle \partial_\mu^* \hat{V}_\mu^+(x) \hat{O}^-(y) \rangle = 0$.

Once ω_V and ω_A are determined, the twist angle ω is obtained by eq. (12). The method described above for determining the twist angle can also be used in case of simulations with partially quenched twisted mass quarks. The estimate of ω is of course affected by $O(a)$ ambiguities. For $\mu \propto \mu_R \neq 0$, $|\omega| = \pi/2$ signals $m_0 = m_{\text{crit}}$.

We determined the twist angle for sets of configurations at $\beta=5.2$, $\mu=0.01$ in the positive and negative quark mass branches; results are reported in fig. 5.

Owing to eq. (6) ω should approach the value $\omega = \pi/2$ from above or below, respectively, when the untwisted quark mass $m_\chi^{PCAC} \propto m_R$ gets close to zero from negative or positive values and $\mu \propto \mu_R$ is kept fixed to a nonzero value. For $\mu = 0.01$, outside the region of metastabilities, we observe a trend of ω consistent with the above expectation (see fig. 5). In the metastability region $(2\kappa)^{-1} = 2.91 - 2.92$ the measured values of ω lie above or below $\pi/2$ in the high or low plaquette phase, respectively, reflecting the behavior of m_χ^{PCAC} in fig. 4. The values of ω are far away from $\pi/2$.

Eqs. (9)-(11) allow to determine the physical currents \hat{V}_μ^a and \hat{A}_μ^a up to the usual multiplicative renormalizations Z_V and Z_A . The physical PCAC quark mass was computed from the Ward identity for the physical axialvector current, analogously to (3)

$$m_q^{\text{PCAC}} \equiv \frac{\langle \partial_\mu^* Z_A^{-1} \hat{A}_\mu^\pm(x) \hat{O}^\mp(y) \rangle}{2 \langle P^\pm(x) \hat{O}^\mp(y) \rangle}. \quad (15)$$

We determined the pion decay constant f_π from the physical axialvector current. The results are plotted in fig. 6 versus the physical PCAC quark mass.

5. Interpretation of the results

The observed metastabilities characterizing co-existing phases with opposite sign of the untwisted quark mass support the picture of a first order phase transition (PT) in the m_0 - μ plane for small values of μ and m_0 close to m_{crit} . Also the

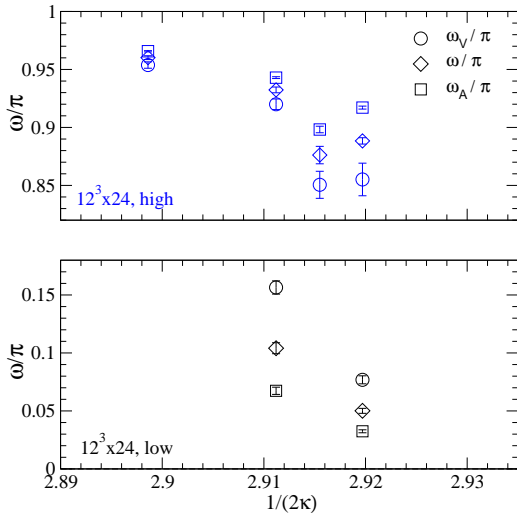


Figure 5. Twist angle as a function of $1/(2\kappa)$ at $\beta = 5.2$ and $\mu = 0.01$ in the two branches.

observed gap in the average plaquette finds a natural explanation [7] in the presence of a first order PT, when the effects of the spontaneous breaking of chirality are considered in combination with the explicit breaking of the symmetry due to the Wilson term in the fermionic action.

A first order PT for Wilson fermions at small $O(a^2)$ quark masses is one of the two possible scenarios predicted by chiral perturbation theory with inclusion of lattice corrections [12] (WChPT). The other one is the well-known Aoki phase, known to be realized at strong gauge couplings (see [13]). Which of the two scenarios applies depends on the sign of the second order ($O(a^2)$) corrections in the effective potential. The generalization of the results of ref. [12] to the case of twisted mass fermions was recently worked out independently in [10,11] and [14]: the first order PT extends to $\mu \neq 0$ getting weaker and weaker for increasing μ ; at the endpoint $\mu_c = O(a^2)$ the PT becomes a critical point.

The metastability of two phases with positive and negative untwisted quark mass has an interpretation, at a microscopic level, in terms of the properties of the eigenvalue spectrum of the Wilson-fermion matrix; studies in this direction are in progress [15] (see [16] for a numerical study

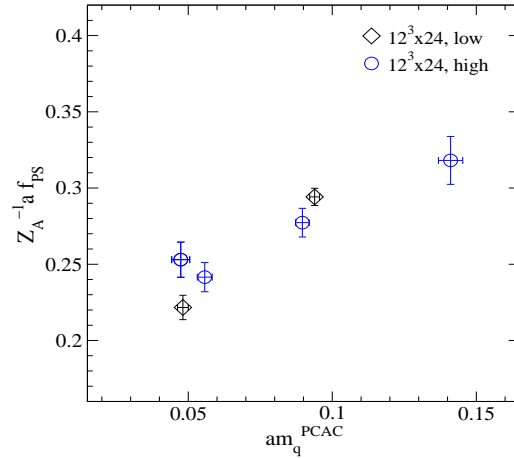


Figure 6. Pseudoscalar decay constant as a function of the physical PCAC quark mass at $\beta = 5.2$ and $\mu = 0.01$ in the two branches.

of the case $\mu=0$). The qualitative picture [15] is that the tunneling between the two phases implies a massive rearrangement of small eigenvalues. This process is suppressed by the zero of the fermion determinant when the eigenvalues move close to the origin in the complex plane. For $\mu \neq 0$ and large enough, the metastability is lifted since the condition $|\mathbf{Im}\lambda| \geq \mu$ implies the depletion of the spectrum around the origin. This conclusion is in agreement with the prediction of twisted mass WChPT (see above).

6. Conclusion and outlook

We investigated the zero temperature phase diagram of twisted mass Wilson fermions. The inclusion of a twisted mass term made it easier to explore the region of small (untwisted) quark masses. Metastabilities, signaled by different values of the plaquette, were visible in this region in thermal cycles and long-living metastable states. The two metastable branches are characterized by opposite values of the untwisted quark mass. The observed phase transition is rather strong: instabilities start already for heavy (~ 740 MeV) pion masses. This is also reflected in the values of the twist angle in the two metastable branches, which are far from $\omega = \pi/2$.

We interpret our findings in terms of the existence of a first order phase transition line in lattice QCD with Wilson fermions; this scenario is supported by Wilson chiral perturbation theory. We argue that a phase transition for small quark masses is accompanied at a microscopic level with the properties of the spectrum of the Wilson-fermion matrix in proximity of the origin in the complex plane.

The existence of a first order phase transition line for small quark masses poses the question, how a critical bare mass can be estimated in practice. One possible choice is to identify m_{crit} with the value of m_0 where the pion mass is minimal. With the untwisted mass set to this value and for $\mu > \mu_c = O(a^2)$ the vacuum is unique.

There are still many aspects which must be clarified in order to get a more detailed picture. First, how the present metastabilities are related with those observed in the literature with different kind of actions and number of flavors [17,6,2] (see also [18] for a recent discussion). We shall start by investigating the influence of the lattice gauge action on the phase structure near zero quark mass [15]. Preliminary results at lattice spacing $a \simeq 0.2$ fm show that replacing the Wilson plaquette action by the DBW2 action makes the minimal pion mass and the jump of the average plaquette substantially smaller.

Another direction of investigation is the dependence of the metastability on the gauge coupling β . In the continuum limit ($\beta \rightarrow \infty$, $a \rightarrow 0$) the minimal pion mass and the jump of the average plaquette are expected to vanish and the first order phase transition line is expected to shrink to a first order phase transition point.

Finally, the most important question is how phenomenology can be done with Wilson fermions in presence of the metastability. In other terms, one has to determine the lightest quark mass that can be simulated in a stable phase, for values of lattice spacings accessible to present simulations.

7. Acknowledgments

F.F. and C.U. would like to thank the *Deutsche Forschungsgemeinschaft* for funding their attendance at the conference.

REFERENCES

1. C. Bernard *et al.*, Nucl. Phys. Proc. Suppl. **106**, 199 (2002).
2. K. Jansen, Nucl. Phys. Proc. Suppl. **129**, 3 (2004); hep-lat/0311039.
3. R. Frezzotti *et al.*, Nucl. Phys. Proc. Suppl. **83** (2000) 941; hep-lat/9909003; R. Frezzotti *et al.*, JHEP **0108** (2001) 058; hep-lat/0101001.
4. R. Frezzotti and G.C. Rossi, JHEP **0408** (2004) 007; hep-lat/0306014; Nucl. Phys. Proc. Suppl. **128** (2004) 193; hep-lat/0311008; R. Frezzotti, talk at this conference.
5. K. Jansen *et al.* [XLF Collaboration], Phys. Lett. B **586**, 432 (2004); hep-lat/0312013; A. Shindler, talk at this conference.
6. JLQCD Collaboration, S. Aoki *et al.*, Nucl. Phys. Proc. Suppl. **106** (2002) 263; hep-lat/0110088.
7. F. Farchioni *et al.*, hep-lat/0406039.
8. M. Hasenbusch, Phys. Lett. **B519** (2001) 177; hep-lat/0107019.
9. G. Münster and C. Schmidt, Europhys. Lett. **66** (2004) 652, hep-lat/0311032; G. Münster, C. Schmidt and E. E. Scholz, hep-lat/0402003.
10. G. Münster, talk at this conference and hep-lat/0407006.
11. L. Scorzato, hep-lat/0407023.
12. S.R. Sharpe and R. Singleton, Jr., Phys. Rev. **D58** (1998) 074501; hep-lat/9804028.
13. E.M. Ilgenfritz *et al.*, Phys. Rev. **D69** (2004) 074511; hep-lat/0309057.
14. S. R. Sharpe and J. M. S. Wu, talk at this conference; hep-lat/0407025; hep-lat/0407035.
15. F. Farchioni *et al.*, work in progress.
16. qq+q Collaboration, F. Farchioni *et al.*, Eur. Phys. J. **C26** (2002) 237; hep-lat/0206008.
17. T. Blum *et al.*, Phys. Rev. **D50** (1994) 3377; hep-lat/9404006.
18. S. Aoki *et al.* [JLQCD Collaboration], hep-lat/0409016.